Testing hadronic-interaction packages at cosmic-ray energies

C. A. García Canal,[1,2] S. J. Sciutto,[1,2] and T. Tarutina[1,*]

[1]*Departamento de Física, Universidad Nacional de La Plata, C.C. 67-1900 La Plata, Argentina*
[2]*IFLP (CONICET), Universidad Nacional de La Plata, C.C. 67-1900 La Plata, Argentina*
(Received 16 July 2008; published 11 March 2009)

A comparative analysis of the secondary particles output of the main hadronic interaction packages used in simulations of extensive air showers is presented. Special attention is given to the study of events with very energetic leading secondary particles, including diffractive interactions.

I. INTRODUCTION

Cosmic ray physics relies strongly on the simulations of air showers [1]. Information on the primary particle energy and mass comes from a hadronic interaction that provides secondary particles with their masses, multiplicities and energies which, unknown in principle, are very difficult to model accurately.

Meanwhile, hard hadronic interactions are well described in the framework of QCD, the soft hadronic interaction observables cannot be calculated from first principles and a combination of empirical parametrization and fundamental theoretical ideas is used to model them. The parametrization constitutes another type of difficulty as the accelerator data are available for much lower energy, another kinematic region and different projectile-target configuration.

In this work we comparatively analyze the hadronic interaction models for very high primary energies. We consider the models included in the packages: SIBYLL2.1 [2,3], QGSJET01c [4], QGSJETII-3 [5], and EPOS1.6 [6], which is the successor of NEXUS [7]. There is an important difference in the way that different models describe hadronic interaction data. In the next section a brief description of these packages will be given.

Because of their importance for cosmic ray shower development, we pay special attention to those particular events characterized by a small number of secondaries that include a leading particle carrying a substantial fraction of the projectile energy. We will call them very energetic leading particle (VELP) events. While a precise definition of VELP events is presented in Sec. III, we can say that most of such events correspond to diffractive processes. From the theoretical point of view, a diffractive process is a high energy hadronic reaction where no quantum numbers are exchanged between the colliding particles [8]. From the point of view of shower development those processes are effective as a way to transport the primary energy deep into the atmosphere, thus influencing the position of the shower maximum X_{max}. This observable is one of the most important parameters in extensive air shower (EAS) physics

and is used to deduce the chemical composition of primary cosmic rays.

In Ref. [9] the three hadronic interaction packages SIBYLL2.1, QGSJET01c, and DPMJET were extensively compared. First, the observables of individual collisions were studied and then the shower development was simulated using SIBYLL2.1 and QGSJET01c. It was found that the relative probability of diffractive processes during the shower development has a non-negligible influence over the longitudinal profile as well as the distribution of muons at ground level. Since that time, new packages of hadronic interactions have been released, namely, QGSJETII-3 and EPOS1.6. Presently, EPOS is widely used in EAS simulations. The appearance of these models motivated us to accomplish a thorough systematic study and comparison of these packages. In this paper, we present the observables generated by SIBYLL2.1, QGSJETII-3, and EPOS1.6 and we also include the results of QGSJET01 for comparison.

This paper is organized as follows: in the next section we review the main features of the different interaction packages; in Sec. III the details of the performed calculations are presented and the results are discussed; Sec. IV contains a summary and our conclusions.

II. HADRONIC INTERACTION MODELS

At intermediate energies soft processes dominate hadron-hadron interactions. The corresponding parton cascades are characterized by a small momentum transfer and therefore, perturbative QCD cannot be applied. Consequently, to describe soft processes an object called phenomenological soft Pomeron was introduced. The amplitude for the Pomeron exchange cannot be calculated from first principles and, therefore, it is postulated and simply parametrized.

As the energy increases, the contribution of another type of processes called semihard which are characterized by the appearance of jets of hadrons with large p_T becomes important. In these processes some partons in the cascade appear with large momentum transfer and the perturbative methods become applicable. The concept of semihard Pomeron was proposed to describe this mechanism [10–12]. It includes the use of a soft Pomeron description for

*tarutina@fisica.unlp.edu.ar

the low virtuality part of the parton cascade and the perturbative QCD techniques for the high virtuality part.

At present, there are two different approaches in use to describe high energy hadronic collisions: (1) the Gribov-Regge Theory (GRT), which employs the soft and semihard Pomeron description [13], and (2) the QCD eikonal (minijet) approach [14,15].

QGSJET01 is based on GRT and the quark-gluon string model. The parton densities used in this model are based on pre-HERA data. The cross section for diffraction dissociation is a constant fraction of the elastic cross section. At present, this model is considered outdated.

At very high energies the number of partonic cascades becomes very large and they start to overlap and interact between each other. These nonlinear effects can be described by Pomeron-Pomeron coupling in the low virtuality region. They are taken into account in QGSJET-II, which is a successor of QGSJET01. The parton densities in this model updated after the analysis of Ref. [9] include the correct behavior for the ratio of diffractive to elastic cross sections, i.e. decreasing with increasing energy.

SIBYLL is based on the minijet approach to describe semihard processes. The new version of SIBYLL, SIBYLL2.1 [3], includes the GRT and takes into account the exchange of multiple soft Pomerons to describe soft processes. To treat nonlinear effects this model assumes that parton densities in the region of small virtualities are completely saturated and that partons are produced for transverse momentum larger than some cutoff that increases with energy. Also the updated parton densities were implemented in the new version of SIBYLL.

EPOS [6] is a recent implementation of GRT. EPOS stands for Energy-conserving quantum mechanical multiple scattering approach, based on Partons (parton ladders), Off-shell remnants, and Splitting of parton ladders. In this model, like in QGSJET, soft and semihard Pomeron amplitudes are used. The nonlinear effects are taken into account by an effective treatment of lowest order Pomeron-Pomeron interaction graphs. This model describes very well detailed RHIC data and other available data from high energy particle physics experiments. In EPOS, energy conservation is considered in both cross section and particle production calculations. An important feature of this model is the explicit treatment of the projectile and the target remnant hadronization which leads to a more complete description of baryon and antibaryon production.

III. CALCULATIONS

The results presented in this paper can be understood as a sort of a quantitative experiment as we analyze the statistical secondary particle information produced by different hadronic packages with the same input parameters and compare them with each other. The input parameters include: (1) the type of primary particle; (2) the type of target; (3) the energy of the primary particle, E_P and (4) the

number of collisions N_{coll}. Because the main component of the air is nitrogen, we choose this nucleus as a representative target for our case of hadronic collisions that occur within the Earth's atmosphere. Typical primary particles are nucleons (proton, neutron) and charged pions; other hadronic projectiles are also possible but their number is substantially smaller in the case of EAS. The energies of the projectiles range from the minimum energy supported by the corresponding models (30 GeV for EPOS and QGSJET, and 100 GeV for SIBYLL), up to the highest cosmic ray energies (≈ 100 EeV).

The number of collisions was determined taking into account (1) the run time of each hadronic package, and (2) the necessity to obtain good enough statistics for further analysis. The SIBYLL package has a shortest running time and the number of collisions for this package was taken to be 10 000. For QGSJET-II we also analyzed 10 000 collisions. For EPOS, 3 000 collisions were analyzed for lower energies, and for high energies, when the number of secondary particles gets very large and therefore the calculation gets very slow, $N_{coll} = 1000$ was taken.

Each secondary particle is characterized by the following: (1) its type, e.g. proton, π^+, etc.; (2) its kinetic energy E_{sec}; and (3) the angle between the primary and the secondary particle direction. All the observables discussed in this work correspond to the laboratory system.

It is known that the secondary particles with small energies (say, less than 40 MeV) do not contribute significantly to the air shower development and are not tracked in EAS simulations; therefore, such particles are excluded from the present analysis.

We separated all collision events into inelastic and those what we call VELP events. As it was already mentioned in the introduction, in this work we are interested in the processes which are effective as a way to transport the energy deep down the atmosphere. To separate the VELP events we apply the following criterion: (1) among the secondaries produced after a given collision with primary energy E_P, the most energetic one is localized and labeled as the "leader" (or leading particle), carrying the energy E_{lead}. (2) The average energy of the rest of the secondaries (those not including the leading particle), $\langle E_{sec} \rangle$, is determined. (3) The leading energy fraction, defined as

$$f_L = \frac{E_{lead}}{E_P}, \tag{1}$$

is then analyzed as follows:
  (i) if $f_L \gtrsim f_1$ the event is labeled as a VELP one (f_1 is a given constant).
 (ii) if $f_2 < f_L < f_1$, (f_2 another given constant) the event is labeled as a VELP one only if $\langle E_{sec} \rangle / E_{lead}$ is larger than a given value g that depends on f_L.
(iii) In any other case the event is labeled as non-VELP or "inelastic collision".

In all our calculations we have taken $f_1 = 0.95$ and $f_2 = 0.3$, and $g(f_L) = 0.01 + 0.6(1 - f_L)^2$. This particular election corresponds to an efficient way of labeling events characterized by a relatively small number of secondaries containing an energetic leading particle capable of contributing considerably to the energy transport deep down in the atmosphere during the air shower development. The VELP events distinguished with the above criterion include most of the standard diffraction events.

To illustrate how our algorithm works we present in Fig. 1 a representative case that corresponds to proton-nitrogen collisions at energy $E_P = 10$ TeV calculated using EPOS (upper row), QGSJET-II (middle row) and SIBYLL (lower row). The VELP events are shown by large red triangles whereas the rest of the events correspond to small green dots. The plots in the left side column represent the N_{sec} versus f_L distributions of the collision events. As it was already mentioned before, all events with $f_L \geq 0.95$
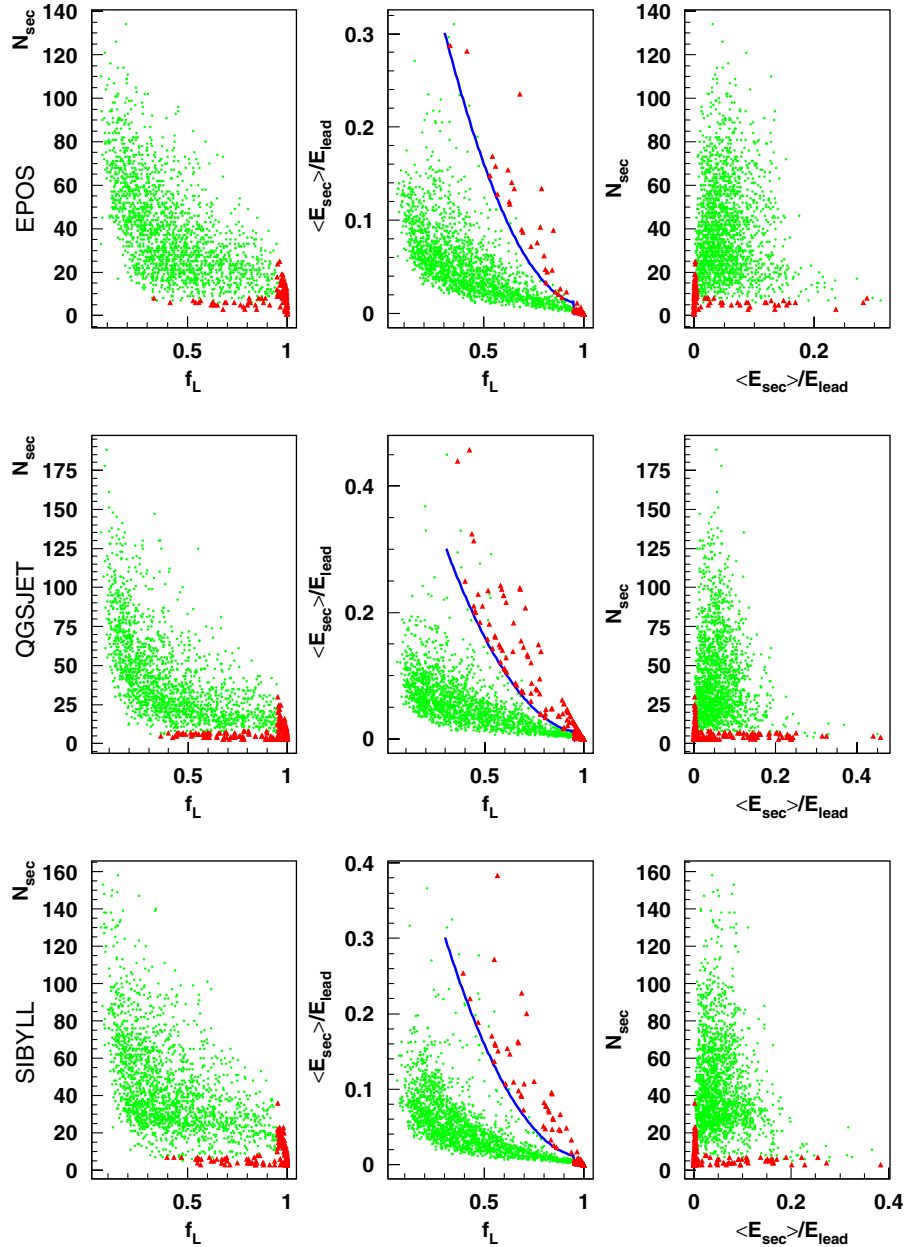

FIG. 1 (color online).   Scatter plots illustrating VELP event selection, produced with sets of 2000 collisions of 10 TeV protons, simulated with EPOS (upper row), QGSJET-II (middle row), and SIBYLL (lower row). The plots in the left side column correspond to N_{sec} versus f_L, while the middle and right side columns correspond to $\langle E_{sec} \rangle / E_{lead}$ versus f_L and N_{sec} versus $\langle E_{sec} \rangle / E_{lead}$, respectively. The large red triangles (small green dots) correspond to VELP (non-VELP) events; the solid line in the middle column plots represents the function $g(f_L)$ (see text).

are marked as VELP. They lie approximately along a straight line and are characterized by a relatively low multiplicity ($N_{sec} \lesssim 20$). When f_L is not that large ($0.3 < f_L < 0.95$) there is a number of events that are characterized by a very low multiplicity ($N_{sec} < 10$) and therefore should be chosen as VELP. These events lie on the approximately straight line parallel to the f_L-axis of the plot. It is important to notice that in the case of EPOS there are very few events with $N_{sec} < 10$ and $0.3 < f_L < 0.95$ compared to case of QGSJET-II and SIBYLL.

On the plots in the middle of Fig. 1 the $\langle E_{sec} \rangle / E_{lead}$ versus f_L distributions are shown. The events with $f_L \gtrsim 0.95$ are characterized by a small value of $\langle E_{sec} \rangle / E_{lead}$ where they concentrate. The VELP events corresponding to $0.3 < f_L < 0.95$ lie above the solid line representing the function $g(f_L)$ defined above. The form of this function was obtained empirically so that the events with low multiplicity and large f_L are VELP's in the simulations with all packages: EPOS, QGSJET-II, and SIBYLL. Notice that above the solid line there are non-VELP events. These are the events where the leading particle possess the quantum numbers different from that of the projectile and therefore they are marked as "inelastic".

The plots on the right side show the N_{sec} versus $\langle E_{sec} \rangle / E_{lead}$ distributions. It is seen that large values of $\langle E_{sec} \rangle / E_{lead}$ correspond to events with low multiplicity.

We start our analysis from the studies of the multiplicity of secondary particles. In Fig. 2 we show the distributions of the number of secondary particles N_{sec} corresponding to events at two energies. The plotted frequency is the number of events with the specific N_{sec} divided by the total number of collisions. One can identify the peak at low N_{sec} as the signature of VELP events. It can be seen that for small N_{sec} the shape of the distribution is different for all models. It is worthwhile mentioning that the data generated with EPOS1.6 does not present a prominent VELP peak for low multiplicity, compared with the other models. At high energies, the distribution gets flatter and the VELP peak is clearly seen, but it is small. From the EPOS1.6 documentation that is available, we cannot find a clear explanation for this different behavior. Nevertheless, we consider that this feature of EPOS could come from the generation of diffractive events that contain a not very reduced number of secondaries.

It is also interesting to compare the energy dependence of averaged multiplicities calculated in different models. In Fig. 3 we show the average number of secondary particles $\langle N_{sec} \rangle$ produced in the collisions as a function of the primary energy. It can be seen that for $E_P > 108$ GeV the difference between the two models becomes significant. At highest energies the largest amount of secondary particles is produced in the QGSJET-II case, clearly larger than the cases of QGSJET01c and EPOS1.6. The least $\langle N_{sec} \rangle$ is given by SIBYLL2.1. For example, at 10 EeV SIBYLL2.1 produces in average approximately 425 sec-
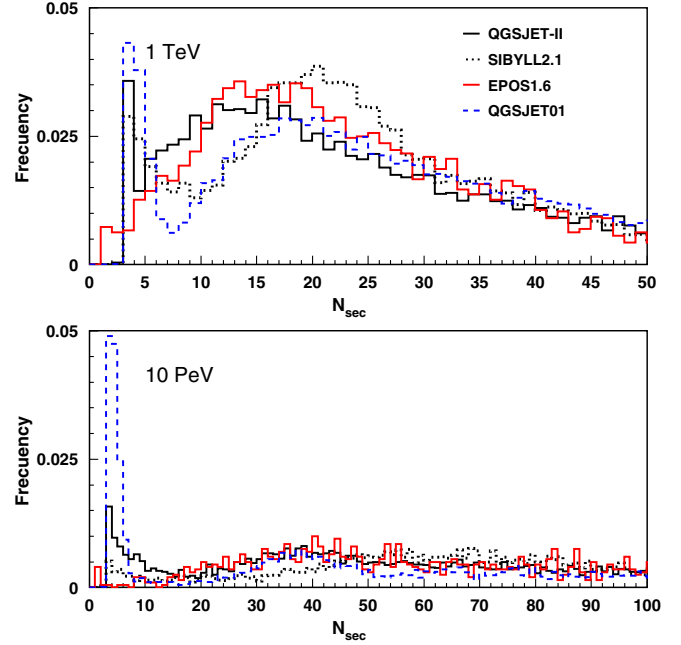

FIG. 2 (color online). Number of secondary particles distributions at two different energies: 1 TeV and 10 PeV for the proton-nitrogen collisions.

ondary particles, EPOS1.6-450, QGSJET01c-675 particles and QGSJETII-3 produces 1225 particles. This high number of secondary particles produced at the highest primary energies is a well known feature of the QGSJET package.

For low energies the largest amount of secondaries is given by QGSJET01c, and then by QGSJETII-3, EPOS1.6,
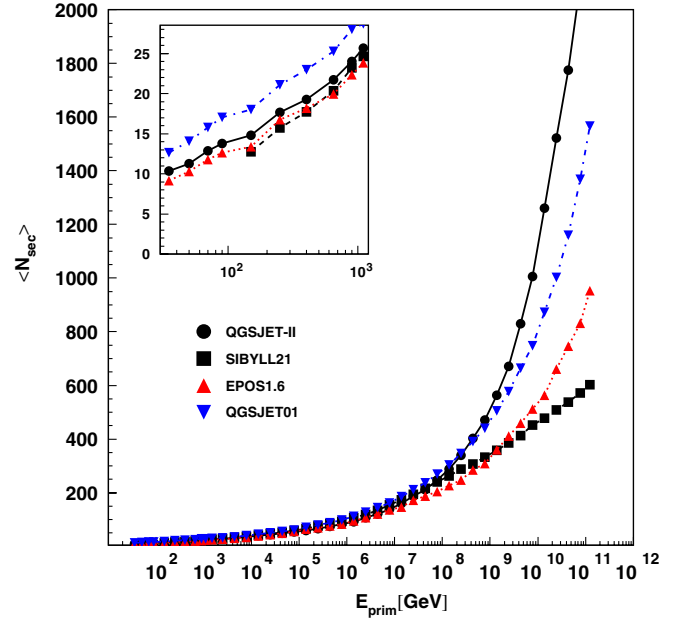

FIG. 3 (color online). The dependence of the mean number of secondary particles ($\langle N_{sec} \rangle$) on the primary energy for the case of proton-nitrogen collisions.
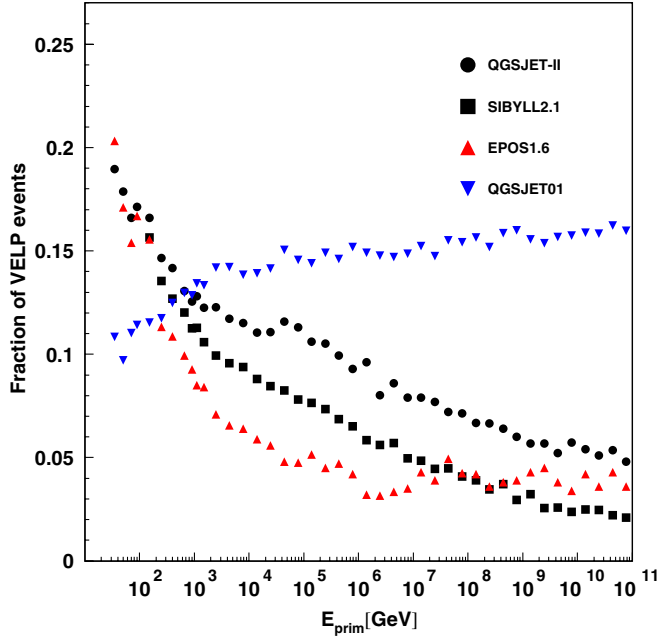
FIG. 4 (color online).   Fraction of VELP events versus primary energy for the case of proton-nitrogen collisions.

and SIBYLL2.1. EPOS1.6 produces more secondary particles than QGSJET-II. But the difference is not as large as in the high energy case.

In Fig. 4 we present the dependence of the fraction of VELP events on the primary energy. The fraction of VELP events is defined as the number of VELP events divided by the total number of events and this quantity is directly related to the diffractive to total cross section ratio.

All the models studied, except QGSJET01c, present a similar shape for the fraction of VELP events: it reduces with the primary energy. On the contrary, as it was already discussed in Ref. [9], QGSJET01c shows a nearly constant dependence. The QGSJETII-3 gives a larger amount of VELP events than SIBYLL2.1 and EPOS1.6. This is expected from the pronounced VELP peak in the multiplicity

distributions generated by QGSJETII-3. As before, for the energy of 1 TeV QGSJET and SIBYLL2.1 give similar results. At the highest energies QGSJETII-3 gives the highest fraction (5.5%), SIBYLL2.1 (3%) the least, EPOS1.6 is in between (4%). EPOS1.6 produces less VELP events for lower energies and shows weaker dependence on energy for high primary energies compared to other models. Indeed, for very high energies the dependence is almost flat.

For very high energies, the information on diffractive to total cross sections ratios obtained from the shower development is of important interest for particle physics because accelerator data is unavailable for this energy range. There are different theoretical models that predict diffractive cross sections and they all differ substantially for very high energies (see, for example, Refs. [16–18] and references therein). Therefore, the cosmic ray data could help to distinguish among these models.

We now turn to the study of the relative amount of different secondary particles produced in the collisions. On Fig. 5 we present the dependence of the fraction of secondary pions, kaons and nucleons on the primary energy. This fraction is defined as the mean number of secondary particles of a given type $\langle N_{sec}^i \rangle$ (where i stands for the particle type) divided by the mean total number of secondary particles $\langle N_{sec} \rangle$.

It can be seen that at the highest energies approximately 80% of all secondary hadrons are pions (neutral and charged). Pions are important for shower development because: (1) charged pions decay into charged muons which are detected by surface detectors; (2) neutral pions decay into gamma quanta and thus initiate electromagnetic showers. It can be seen that SIBYLL2.1, QGSJETII-3 and EPOS1.6 produce similar results, that is a pion fraction that increases with energy and saturates at the highest primary energies. At 10^{11} GeV SIBYLL2.1 and QGSJETII-3 produce virtually identical results, that are 7% larger than the EPOS1.6 fraction. On the other hand, QGSJET01 predicts a fraction of pions that decreases with energy.
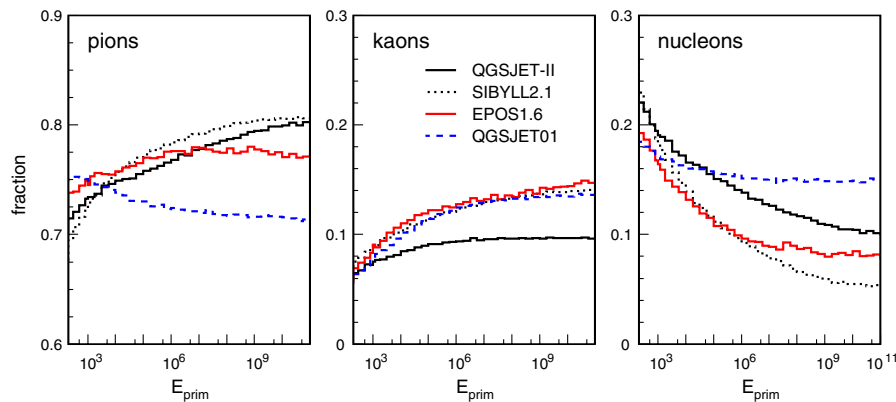

FIG. 5 (color online).   The dependence of the fraction of secondary pions, kaons and nucleons on the primary energy in the case of proton-nitrogen collisions.

Kaons also play a significant role in shower development (neutral kaons decay into neutral pions and charged kaons decay into charged pions, which in turn decay into detectable muons) and it is thus worthwhile studying their production rates. All models produce kaon fractions slowly increasing with energy. At the highest energies, kaons represent approximately 14% (QGSJETII-3 gives 10%) of all secondaries.

The right hand panel of Fig. 5 shows the dependence of the secondary nucleon and antinucleon fraction on the primary energy. It can be seen that the fraction of such particles reduces with primary energy. In our analysis we see that the largest amount of baryons is produced by the QGSJETII-3 package (10%), the least is given by SIBYLL2.1 (5%) and EPOS1.6 (8%) is in between of both. It can be seen that QGSJETII-3 produces more nucleons than SIBYLL2.1 and EPOS1.6.

Figure 6 shows the relative amount of pions and kaons separated by charge for QGSJETII-3, SIBYLL2.1, and EPOS1.6. We show the energy dependence of the relative fractions of π^-, π^0, π^+ and K^-, K_S^0, K_L^0, K^+.

Notice that the fraction of pions of each type is defined as its mean multiplicity divided by the total mean multiplicity of pions; and similarly the K^-, K_S^0, K_L^0, K^+ fractions add up to 1.

It is seen that 38% of all pions are neutral pions. The relative amount of neutral kaons does not change with primary energy. At high energies the amount of π^- and π^+ becomes equal (31% of all pions). At lower energies there are more π^+ than π^-. There are no important differences between different models with respect of the multiplicity of different charges of pions.

In the case of kaons, it is found that at high energies each type of kaons contribute 25% to total kaon multiplicity. The fractions of K_S^0 and K_L^0 do not change significantly with energy. At lower primary energies, there are more K^+ than K^-. The models differ with respect to the slope of energy dependence of the fractions of K^- and K^+.

On Fig. 7 we show the relative fractions of secondary neutrons, antineutrons, protons and antiprotons as a func-tion of the primary energy. These fractions are defined as the mean multiplicity of the particle of each charge divided by the total mean multiplicity of nucleons and antinucleons. We recall that in the analysis of these secondaries, we have excluded all particles with kinetic energy less than 40 MeV, due to their irrelevance in the case of air shower development. Such low-energy particles are, in general, nucleons.

It can be seen that the amounts of neutrons and protons decrease with energy, whereas the amounts of antineutrons and antiprotons increase. Notice that at the highest energies both QGSJETII and SIBYLL2.1 produce similar amounts, i.e. 25% approximately, of n, $\overline{n}$, p, $\overline{p}$; this is not the case of EPOS1.6 (see below).

The slopes of the plots produced in three models are different from each other. EPOS1.6 shows the largest separation between the fractions of nucleons and antinucleons at high energies and for all energies EPOS produces more neutrons and less antineutrons. Namely, at high energies EPOS1.6 produces approximately 30% more neutrons and 70% less antineutrons than, for example, SIBYLL2.1. For secondary protons and antiprotons the situation is different. For low energies, EPOS1.6 produces less protons compared to SIBYLL2.1 and QGSJETII-3. At high energies ($E_p > 500$ PeV), EPOS1.6 gives slightly more protons than SIBYLL2.1 and QGSJETII-3. Notice also that in the QGSJETII-3 and SIBYLL cases and for all energies the fraction of antineutrons is larger than the corresponding one for antiprotons. This contrasts with the EPOS1.6 case where the fraction of antiprotons is larger than the fraction of antineutrons.

Now we turn our attention to the energy of secondary particles produced in proton-nitrogen collisions. We study the fraction of interaction energy carried by secondary particles. This fraction is defined as the mean energy carried by secondary particles of a certain type divided by the primary energy.

In Fig. 8 we compare the fraction of mean secondary energy carried by pions, kaons and nucleons. Generally these plots follow the behavior of the mean multiplicity of
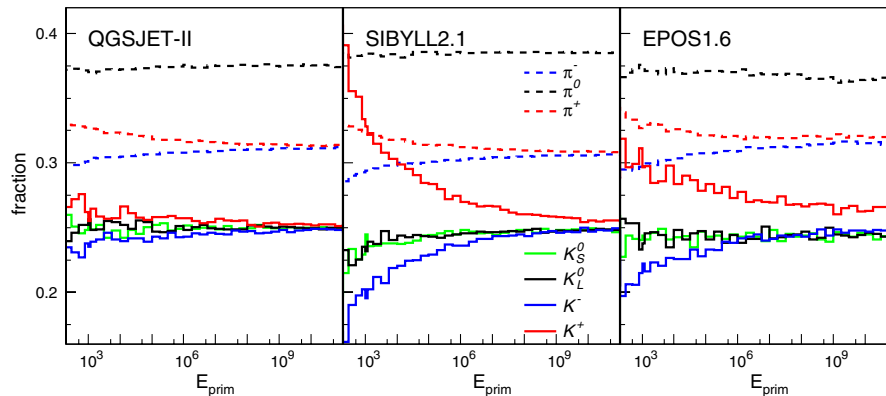

FIG. 6 (color online). The dependence of the fraction of secondary pions and kaons separated by charge on the primary energy in the case of proton-nitrogen collisions.
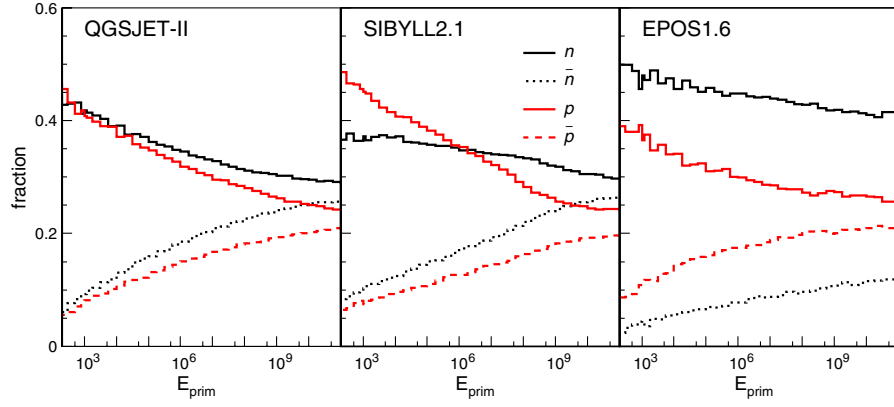
FIG. 7 (color online).   The dependence of the fraction of secondary nucleons separated by charge on the primary energy in the case of proton-nitrogen collisions.

pions, kaons and nucleons presented in Fig. 5. That is, the relative amount of energy and the general shape of the primary energy dependence are dictated by multiplicity plots.

The mean multiplicity of pions increases with energy and consequently increases the amount of energy carried by pions and the same is true for kaons. The mean multiplicity of nucleons decreases with primary energy and the fraction of interaction energy decreases as well.

Notice that the major part of the interaction energy is carried by pions which is expected from the fact that the majority of secondary particles are pions. Pions produced in QGSJETII-3 carry the largest amount of energy compared to other models. At largest energies pions carry approximately 60% (QGSJET23), 55% (QGSJET01c), 50% (SIBYLL2.1), and 45% (EPOS1.6).

In EPOS case, kaons take away approximately 5% more energy than in other models. For example, at the largest energies, the kaons produced by EPOS1.6 carry approximately 15% of the primary energy, in contrast with 10% for QGSJETII-3 or SIBYLL2.1 or QGSJET01c.

At highest energies nucleons produced in SIBYLL2.1 carry approximately 30% of energy, QGSJETII-3 and

QGSJET01c-23% and in EPOS1.6 20%. For all primary energies the amount of energy carried by nucleons produced in EPOS1.6 is the smallest.

On the next two figures we present the fractions of interaction energy carried by secondary mesons and nucleons separated by charge.

In Fig. 9 we show the fraction of mean secondary energy carried by mesons: pions and kaons generated in QGSJETII-3 (left panel), SIBYLL2.1 (middle panel) and EPOS1.6 (right panel). As before, the fraction of interaction energy carried by the particles of each type is defined as the total energy carried by these particles divided by the primary energy.

As expected from the multiplicity plots, the largest fraction of energy is carried by neutral pions and its value increases with primary energy. The curves for charged pions calculated using EPOS160 present almost flat dependence.

In the case of kaons, all kaons show the same energy dependence slowly increasing with energy. Only the fraction of interaction energy carried by K^+ calculated by SIBYLL2.1 decreases with energy. This can be explained
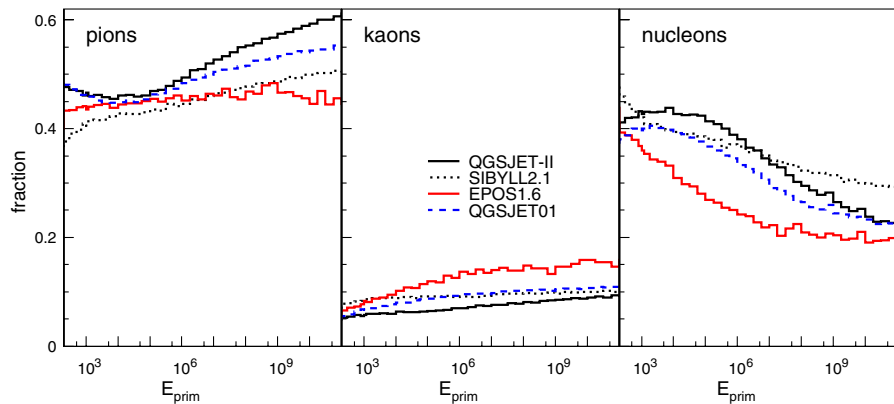

FIG. 8 (color online).   Fractions of interaction energy carried by secondary pions, kaons and nucleons as a function of the primary energy in the case of proton-nitrogen collisions.
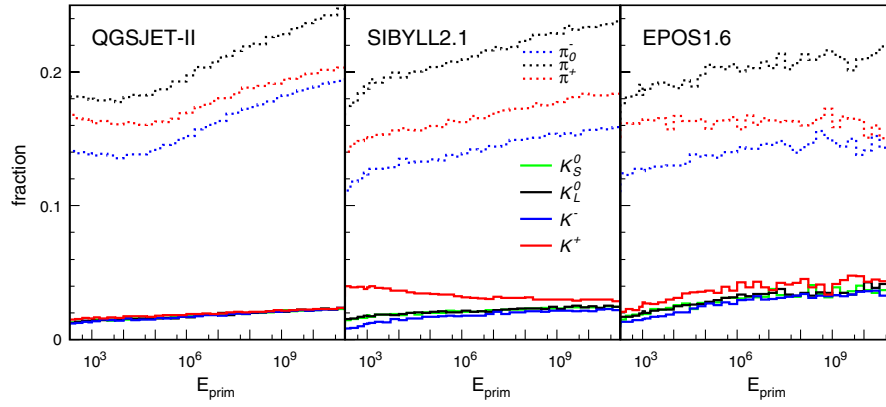
FIG. 9 (color online).   Fractions of interaction energy carried by different secondary mesons as a function of the primary energy in the case of proton-nitrogen collisions.

by the large multiplicity of positively charged kaons generated in this package.

In Fig. 10 we show the fraction of mean secondary energy carried by neutrons, antineutrons, protons and antiprotons generated in QGSJETII-3 (left panel), SIBYLL2.1 (middle panel) and EPOS1.6 (right panel).

In all models, the largest amount of energy is carried by protons. This is expected from the fact that proton is a projectile. Neutrons carry smaller fraction of interaction energy and antiprotons and antineutrons carry very small fraction of interaction energy.

The fraction of interaction energy decreases with primary energy for protons and neutrons and slowly increases for antiprotons and antineutrons. This is in accordance with the multiplicity plots for baryons.

It is seen that in the case of EPOS1.6, protons and neutrons carry the same fraction of interaction energy for $E_{\text{prim}} > 10$ PeV. Generally, all models give similar values of fraction of interaction energy carried by neutrons. For protons, there is a difference between models. For all energies, the protons generated in EPOS carry less inter-

action energy. This can be explained by less amount of VELP events seen in EPOS1.6.

In Fig. 11 we show the distribution of the leading energy fraction f_L for two values of the primary energy, namely, 1 TeV and 10 EeV. f_L distributions are important when one wants to separate the VELP events from the ''inelastic'' collisions. For clarity, we compare only the results of QGSJETII-3 and EPOS1.6. There are two peaks in this distribution. Most of the VELP events come from the relatively sharp peak at $f_L = 1$, which corresponds to the existence of a leading particle among few secondaries which carries almost all available energy. The second peak is wide and its position changes with energy. As the primary energy increases, the number of secondary particles grows and the wide maximum of the distribution shifts towards $f_L = 0$. It is seen from this plot that at 10 EeV, QGSJETII-3 has a maximum very close to $f_L = 0$, which can be explained by the very large number of relatively low-energy secondaries generated in this package. At low energies, the VELP peak is less pronounced. As the energy goes up, the peak generated by all models becomes more
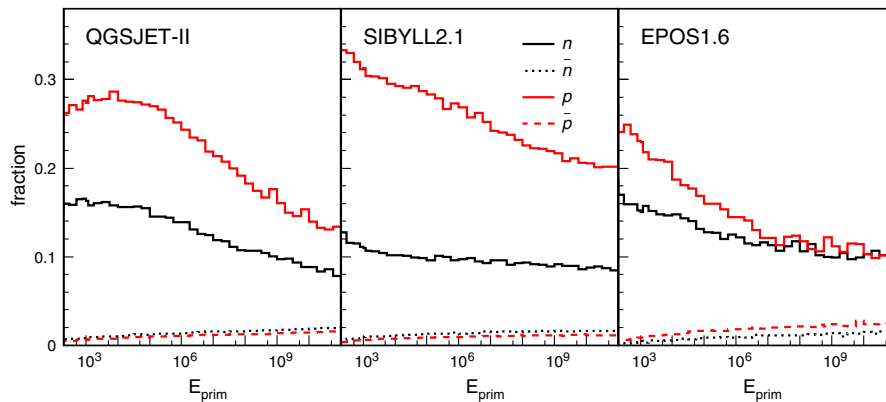

FIG. 10 (color online).   Fractions of interaction energy carried by secondary nucleons as a function of the primary energy in the case of proton-nitrogen collisions.
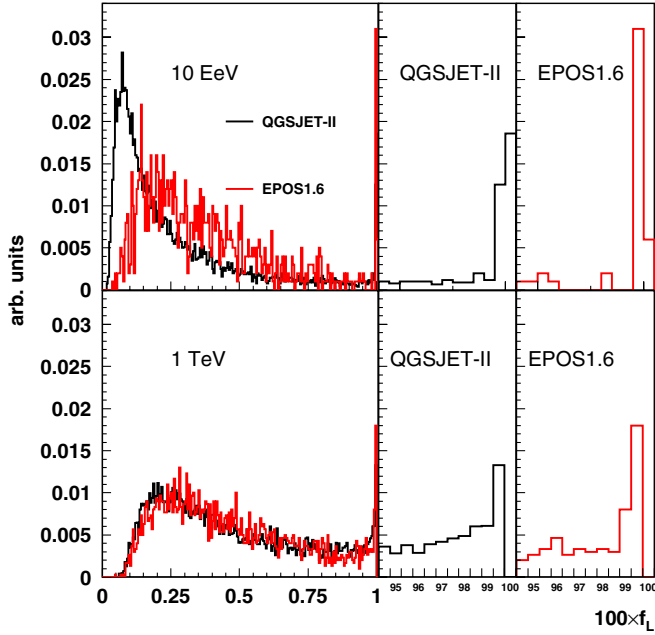
FIG. 11 (color online). Leading energy fraction distributions for proton-nitrogen collisions at $E_{prim} = 10$ EeV (upper panel) and $E_{prim} = 1$ TeV (lower panel).
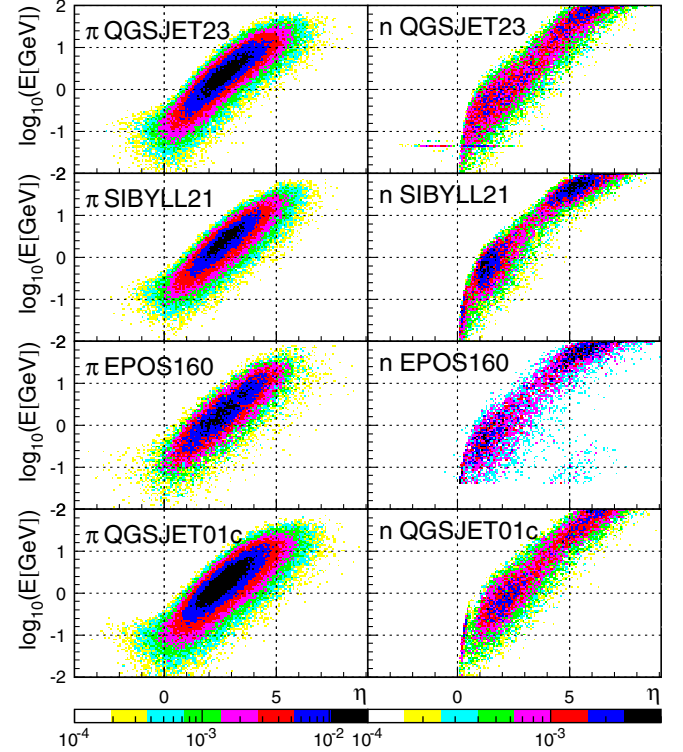

FIG. 12 (color online). Pseudorapidity of secondary pions (left column) and nucleons (right column) versus their energy for the case of proton-nitrogen collisions at 1 TeV. Note different scale for pions and nucleons.

pronounced, and at highest energies EPOS1.6 produces the tallest peak corresponding to VELP events.

We conclude this section with the study of the pseudo-rapidity distributions of secondary particles. They are important in cosmic ray physics because they are significantly correlated with the lateral distributions of muons at large distances from the core. Pseudorapidity is defined by $\eta = -\ln\tan\frac{\Theta}{2}$, where Θ is the angle that specifies the direction of motion of a secondary particle with respect to the direction of the primary particle. Using the pseudorapidity allows to distinguish the secondary particles by their direction of motion with respect to the primary particle, which is important for air shower development.

In Fig. 12 we present the $\eta \times E_{sec}$ two-dimensional distributions for proton-nitrogen collisions at 1 TeV. The left panels show the distributions of the secondary pions and the right panels those of secondary nucleons.

The most outstanding characteristic of the plots in Fig. 12 is the clear linear behavior of the mean pseudorapidities at a given energy with the logarithm of the secondary energy. The slopes of the corresponding lines are similar for all models.

In the case of pions (left hand side plots) the distributions possess a simple structure. The pseudorapidity distributions at a fixed secondary energy are approximately Gaussians with energy independent standard deviation.

The distributions for nucleons present two peaks, consequence of the bimodal energy spectra of secondary nucleons, that is characteristic of all hadronic models [9]. In all models the pseudorapidity distributions in the zones where η is around zero, or negative (recoiling particles) are

somewhat unnatural (see right hand column of Fig. 12), presenting a relative abundance of particles with positive but very small η, and zero recoiling particles ($\eta < 0$) [19]. EPOS1.6 distributions for nucleons also indicate the existence of low-energy secondaries in the near forward direction ($\eta > 4$). From the available EPOS1.6 documentation we cannot find any explanation for such particles.

IV. CONCLUSIONS AND OUTLOOK

We have performed a comparative analysis of secondary particle observables produced in collisions generated by different hadronic packages. We studied the secondary particle information generated by SIBYLL2.1, QGSJETII-3, and EPOS1.6 using identical input data: projectile and target type and primary energy. For comparison with previous analysis, we also included the results of QGSJET01c, even if this package is already considered outdated.

The choice of studied quantities was dictated by their importance for the air shower development. We studied multiplicity distributions of secondary particles, mean multiplicity, inelasticity, fraction of secondary pions and baryons, energy distributions of secondary particles and pseudorapidity distributions. It was shown that the studied models present significant differences for all energy ranges.

We introduced the notion of VELP events, corresponding to events that are characterized by a small number of secondaries and that include a leading particle that carries a substantial fraction of the projectile energy. These events in their majority correspond to the standard diffractive events.

It is seen that QGSJETII-3 produces a very large amount of secondary particles at high energies, twice as much as EPOS1.6. Also, the multiplicity distributions show a different shape for the VELP peak in the case of EPOS1.6 where the peak is small compared to the results generated by other packages.

Because of their importance for shower development, a special attention was given to VELP processes. Our results for the fraction of VELP events at the highest energy are: QGSJETII-3 gives the highest fraction (5.5%), SIBYLL2.1 (3%) the least, and EPOS1.6 is in between (4%). Our analysis gives larger values for the fraction of VELP events than those obtained in Ref. [9]. The primary energy dependence of the fraction of VELP events becomes almost flat at high energies. This implies the almost constant diffractive to total cross section ratio for high energies. For lower energies EPOS generates less VELP collisions when compared to the other models.

Our analysis has shown that EPOS1.6 generates less pions than the other packages (7% less than SIBYLL2.1 at 10 EeV). Another feature of EPOS1.6 is the fraction of secondary neutrons and antineutrons: our calculation gives 30% more neutrons and 70% less antineutrons at $E_P = 10^5$ GeV.

The next step in this analysis is the study of the impact of different models of hadronic interactions on common air shower observables [20]. To simulate air shower development the AIRES program [21] is being used with QGSJETII-3 and EPOS1.6 packages for the generation of hadronic interactions.

ACKNOWLEDGMENTS

[1] J. Knapp, D. Heck, S. J. Sciutto, M. T. Dova, and M. Risse, Astropart. Phys. **19**, 77 (2003).

[2] R. S. Fletcher *et al.*, Phys. Rev. D **50**, 5710 (1994).

[3] R. Engel, T. K. Gaisser, T. Stanev, and P. Lipari, in *Proc. 26th Int. Cosmic Ray Conf.* (Salt Lake City USA, 1999), Vol. 1, p. 415.

[4] N. N. Kalmykov *et al.*, Nucl. Phys. B, Proc. Suppl. **52**, 17 (1997).

[5] S. Ostapchenko, Phys. Rev. D **74**, 014026 (2006).

[6] K. Werner, F. M. Liu, and T. Pierog, Phys. Rev. C **74**, 044902 (2006); arXiv:hep-ph/0506232.

[7] H. J. Drescher, M. Hladik, S. Ostapchenko, T. Pierog, and K. Werner, Phys. Rep. **350**, 93 (2001).

[8] V. Barone and E. Predazzi, *High-Energy Particle Diffraction* (Springer, New York, 2002).

[9] R. Luna, A. Zepeda, C. A. García Canal, and S. J. Sciutto, Phys. Rev. D **70**, 114034 (2004).

[10] N. N. Kalmykov, S. S. Ostapchenko, and A. I. Pavlov, Bulletin of the Russian Academy of Sciences Physics **58**, 1966 (1994); Nucl. Phys. B, Proc. Suppl. **52**, 17 (1997).

[11] H. J. Drescher *et al.*, J. Phys. G **25**, L91 (1999).

[12] S. Ostapchenko *et al.*, J. Phys. G **28**, 2597 (2002).

[13] V. N. Gribov, Sov. Phys. JETP **26**, 414 (1968); **29**, 483 (1969).

[14] T. K. Gaisser and F. Halzen, Phys. Rev. Lett. **54**, 1754 (1985); G. Pancheri and Y. Srivastava, Phys. Lett. B **159**, 69 (1985).

[15] L. Durand and H. Pi, Phys. Rev. Lett. **58**, 303 (1987); Phys. Rev. D **38**, 78 (1988).

[16] E. Gotsman, E. M. Levin, and U. Maor, Phys. Lett. B **347**, 424 (1995); arXiv:hep-ph/9407227.

[17] A. B. Kaydalov, V. A. Khoze, A. D. Martin, and M. G. Ryskin, Eur. Phys. J. C **33**, 261 (2004); arXiv:hep-ph/0311023.

[18] S. M. Troshin and N. E. Tyurin, Eur. Phys. J. C **39**, 435 (2005).

[19] The set of nucleons of energy 47 MeV produced by QGSJETII-3 that have a strange η behavior (clearly visible in the upper right plot of Fig. 12) is assumed to be associated with a package bug and not considered in our analysis.

[20] S. J. Sciutto and T. Tarutina (unpublished).

[21] S. J. Sciutto, in *Proceedings of the 27th ICRC, Hamburg, 2001* (Copernicus Gesellschafr, Hamburg, 2001), Vol. 1, p. 237; see also http://www.fisica.unlp.edu.ar/auger/aires.